Published in final edited form as:
Sci Transl Med. 2012 April 18; 4(130): 130ra47. doi:10.1126/scitranslmed.3003552.

Patient-Specific Induced Pluripotent Stem Cell as a Model for Familial Dilated Cardiomyopathy

Ning Sun[1,2,3,*], **Masayuki Yazawa**[4,*], **Jianwei Liu**[5], **Leng Han**[1,2], **Veronica Sanchez-Freire**[1,2], **Oscar J. Abilez**[6], **Enrique G. Navarrete**[2], **Shijun Hu**[1,2], **Li Wang**[1,2,3], **Andrew Lee**[1,2,3], **Aleksandra Pavlovic**[1], **Shin Lin**[1], **Rui Chen**[7], **Roger J. Hajjar**[8], **Michael P. Snyder**[7], **Ricardo E. Dolmetsch**[4], **Manish J. Butte**[5], **Euan A. Ashley**[1], **Michael T. Longaker**[3,9], **Robert C. Robbins**[10], and **Joseph C. Wu**[1,2,3,10]

[1]Department of Medicine, Division of Cardiology, Stanford University School of Medicine, Stanford, California 94305, USA

[2]Department of Radiology, Stanford University School of Medicine, Stanford, California 94305, USA

[3]Institute for Stem Cell Biology and Regenerative Medicine, Stanford University School of Medicine, Stanford, California 94305, USA

[4]Department of Neurobiology, Stanford University School of Medicine, Stanford, California 94305, USA

[5]Department of Pediatrics, Division of Immunology, Stanford University School of Medicine, Stanford, California 94305, USA

[6]Department of Surgery, Division of Vascular Surgery, Stanford University School of Medicine, Stanford, California 94305, USA

[7]Department of Genetics, Stanford University School of Medicine, Stanford, California 94305, USA

[8]Department of Gene and Cell Medicine, Mount Sinai Medical Center, Stanford University School of Medicine, Stanford, California 94305, USA

[9]Department of Surgery, Division of Plastic and Reconstructive Surgery, Stanford University School of Medicine, Stanford, California 94305, USA

[10]Stanford Cardiovascular Institute, Stanford University School of Medicine, Stanford, California 94305, USA

Abstract

Correspondence: Joseph C. Wu, MD, PhD, Lorry I. Lokey Stem Cell Research Building, 265 Campus Drive, Rm G1120B, Stanford, CA 94305-5454, joewu@stanford.edu.
*Contributed equally

Author contributions: N.S. performed reprogramming, established iPSCs, characterizations, differentiation, MEA assays, Ca^{2+} imaging, project planning, experimental design, data analysis, and preparation of manuscript; M.Y. performed patch clamping, Ca^{2+} imaging, experimental design, data analysis, and preparation of manuscript; E.G.N. performed MEA assays, data analysis, and preparation of manuscript; V.S-F., S.H., L.W., L.H., R.C., A.L., and O.J.A. performed experimental work; J.L. performed AFM; R.E.D, A.P., and M.B. analyzed data and prepared manuscript; E.A.A, R.J.H., M.T.L., R.C.R. and J.C.W. designed experiments and prepared manuscript.

Competing interests: The authors have no competing interests.

Accession numbers: The microarray data can be found at GEO with accession number GSE35108.

Dilated cardiomyopathy (DCM) is the most common cardiomyopathy, characterized by ventricular dilatation, systolic dysfunction, and progressive heart failure. DCM is the most common diagnosis leading to heart transplantation and places a significant burden on healthcare worldwide. The advent of induced pluripotent stem cells (iPSCs) offers an exceptional opportunity for creating disease-specific models, investigating underlying mechanisms, and optimizing therapy. Here we generated cardiomyocytes (CMs) from iPSCs derived from patients of a DCM family carrying a point mutation (R173W) in the gene encoding sarcomeric protein cardiac troponin T. Compared to the control healthy individuals in the same family cohort, DCM iPSC-CMs exhibited altered Ca^{2+} handling, decreased contractility, and abnormal sarcomeric α-actinin distribution. When stimulated with β-adrenergic agonist, DCM iPSC-CMs showed characteristics of failure such as reduced beating rates, compromised contraction, and significantly more cells with abnormal sarcomeric α-actinin distribution. β-adrenergic blocker treatment and over-expression of sarcoplasmic reticulum Ca^{2+} ATPase (Serca2a) improved DCM iPSC-CMs function. Our study demonstrated that human DCM iPSC-CMs recapitulated to some extent the disease phenotypes morphologically and functionally, and thus can serve as a useful platform for exploring molecular and cellular mechanisms and optimizing treatment of this particular disease.

INTRODUCTION

Dilated cardiomyopathy (DCM) is a cardiac disease characterized by ventricular dilatation and systolic dysfunction (1). DCM is the most common cause of heart failure after coronary artery disease and hypertension, and is the leading indication for heart transplantations (2–3). The cost for management of DCM in the US alone has been estimated at between $4 and $10 billion (3). Mutations in genes encoding sarcomeric, cytoskeletal, mitochondrial, and nuclear membrane proteins, as well as proteins involved in Ca^{2+} metabolism, are linked to approximately a third to half the cases of DCM (4–6). Cardiac troponin T (cTnT) is one of the 3 subunits of the troponin complex (Troponin T, C, and I) that regulate the sarcomeric thin filament activity and muscle contraction in cardiomyocytes (CMs). cTnT is essential for sarcomere assembly, contraction, and force production (7). Mutations in the cardiac troponin T gene (TNNT2) often lead to DCM (8) and are frequently expressed as a malignant phenotype with sudden cardiac death and heart failure at an early age (9–10). *In vitro* biochemical studies have found that decreased Ca^{2+} sensitivity and/or ATPase activity, which impair force production, may be the underlying mechanisms for certain TNNT2-mutation induced DCM (9,11–14). Mouse models of TNNT2 mutations recapitulate the human DCM phenotype, providing extensive insight into the possible mechanisms of the disease (11–12). The contribution of mouse models in the overall understanding of DCM has been enormous. However, several important differences exist between the mouse and human models. For example, the mouse resting heart rate is approximately 10-fold faster than human's. The electrical properties, ion channel contributions, and cardiac development of mouse CMs are all differ from those of human. Unfortunately, cardiac tissues from DCM patients are difficult to obtain and do not survive in long-term culturing. With the advent of induced pluripotent stem cells (iPSCs) (15–16), functional CMs can be differentiated from human iPSCs (17–18). Patient-specific iPSC-CMs such as the long QT syndrome, Leopard syndrome, and Timothy syndrome have been shown to recapitulate human cardiovascular diseases and enable the testing and optimization of empirical therapies (19–22). Thus, a human DCM iPSC-CM model would be an important complement to mouse models for understanding the cellular and physiological processes of DCM as well as for drug screening in human cells.

Here we generated iPSC-CMs from a three-generation family of DCM patients carrying a point mutation (R173W) in exon 12 of the TNNT2 gene. We studied the morphology and function of DCM iPSC-CMs, recorded their electrophysiology with patch clamping and

microelectrode arrays (MEAs), assessed Ca^{2+} handling with Ca^{2+} transient analysis, and quantified contractile force production using atomic force microscopy (AFM). Compared to the controls, iPSC-CMs derived from DCM patients displayed a consistent increased heterogeneous sarcomeric organization at early stage post differentiation, consisting of a more severe punctate distribution of sarcomeric α-actinin. Individual DCM iPSC-CMs also exhibited altered Ca^{2+} handling compared to controls. β-Adrenergic stimulation increased the number of iPSC-CMs with abnormal sarcomeric α-actinin distribution, compromised contractility, and induced failure of spontaneous contraction. Importantly, we demonstrated that treatment with β1-selective β-blocker (metoprolol) improved the sarcomeric organization, whereas over-expression with sarcoplasmic reticulum Ca^{2+} ATPase (Serca2a) markedly increased the contractile force and improved Ca^{2+} handling in DCM iPSC-CMs. In summary, our results show that DCM iPSC-CMs to some extent recapitulated the disease phenotype, and therefore can be a useful tool for investigating the disease mechanisms involved understanding DCM and drug screening, as well as optimizing medical management.

RESULTS

DCM family with a disease-associating point mutation (R173W) in TNNT2

We recruited a cohort of seven individuals from a DCM proband carrying an autosomal dominant point mutation on exon 12 of the gene TNNT2, which causes an Arginine (R) to Tryptophan (W) mutation at amino acid position 173 in the protein cTnT. The potential causal effect for DCM of this particular point mutation was confirmed by genetic screening of a panel of 17 primary DCM associated genes, *in silico* analysis (Table S1), and genetic co-segregation studies (Fig. S1). A mutation at the same amino acid position (R173G) was also reported in a completely unrelated Belgian family with DCM (23), suggesting a strong association of this particular locus with the disease. The seven recruited individuals covered 3 generations (I, II, and III) (Fig. 1A). Four patients (Ia, IIa, IIb, and IIIa) were confirmed to carry the TNNT2 R173W mutation in one of the two alleles by PCR amplifying the genomic locus of TNNT2 and DNA sequencing, while the other 3 individuals (Ib, IIc, and IIIb) were confirmed normal and served as controls in the subsequent studies (Fig. 1B and Fig. S1). All four patients who carry the specific R173W mutation manifested clinical DCM symptoms with dilated left ventricle and decreased ejection fraction, and were treated medically (Table S2). A 14-year-old diseased patient (IIIa) had an orthotopic heart transplant due to severe clinical symptoms.

Generation and characterization of patient-specific iPSCs

To generate patient-specific iPSCs, skin fibroblasts were expanded from skin biopsies taken from each individual (Fig. 1C) and reprogrammed with lentiviral Yamanaka 4 factors (*Oct4, Sox2, Klf4*, and *c-MYC*) under feeder-free condition. Colonies with TRA-1-60^{+} staining and human embryonic stem cell (hESC)-like morphology (Fig. 1, D and E) were selected, expanded, and established as individual iPSC lines. For each individual, 3–4 iPSC lines were established for subsequent analyses. All of the DCM iPSC lines were confirmed to contain the specific R173W mutation by genomic PCR and DNA sequencing (Fig. S2). All established iPSC lines expressed the pluripotency markers Oct4, Nanog, TRA-1-81, and SSEA-4, and were positive for alkaline phosphatase (Fig. 1F). Microarray analyses indicated these iPSC lines were distinct from the parental skin fibroblasts, expressing a global gene pattern more similar to hESCs (Fig. S3A). Quantitative bisulphite sequencing showed that the promoter regions of Oct4 and Nanog were hypomethylated in all the tested iPSC lines, indicating active transcription of the pluripotency genes (Fig. 1G). The established iPSC lines maintained a normal karyotype after extended passage (Fig. S3B), with the majority of them exhibiting silencing of exogenous transgenes and re-expression of endogenous Nanog

(Fig. S4). iPSC lines with incomplete transgene silencing were removed from the subsequent studies. These patient-specific iPSCs were able to differentiate *in vitro* into cells of all three germ layers (Fig. S5) and subsequently formed teratomas upon injection into the kidney capsules of immunodeficient mice (Fig. 1H).

Baseline electrophysiology of DCM iPSC-derived beating embryoid bodies (EBs)

We next differentiated the DCM iPSCs into the cardiovascular lineage using a well-established 3D differentiation protocol developed by Yang *et al.* (24). Two iPSC lines from each individual were selected for differentiation into spontaneous beating EBs and for subsequent functional analyses (Table S3). Spontaneous beating was observed as early as day 8 post differentiation. The efficiency of differentiation to cardiac lineage varied among different lines (Fig. S6A, Videos S1 and S2). Beating EBs derived from control and patient iPSCs contained approximately 50–60% cTnT-positive CMs (Fig. S6, B and C). Allele-specific reverse transcriptase (RT)-PCR of beating EBs derived from three iPSC clones of 3 DCM patients indicated bi-allelic expression of the wild type and mutant (R173W) TNNT2 gene (Fig. S7). The beating EBs from the control and DCM iPSCs 18–48 days post differentiation were seeded on multi-electrode array (MEA) probe (Fig. S8A and Video S3) and their electrophysiological properties recorded (Fig. S8B). Both control (n=45) and DCM (n=57) iPSC-derived beating EBs exhibited comparable beat frequencies, field potentials, interspike intervals, and field potential durations (FPD) at baseline (Table S4 and Fig. S8C).

TNNT2 R173W DCM iPSC-CMs exhibit an increased heterogeneous sarcomeric organization pattern

We next dissociated the beating EBs into small beating clusters and single beating CMs for further analysis (Videos S4 to S7). The organization of myofibrils in the iPSC-CMs was assessed by immunocytochemistry. Both control and DCM iPSC-CMs expressed sarcomeric proteins cTnT, sarcomeric α-actinin, and myosin light chain 2a (MLC2a), as well as the cardiac gap junction protein connexin 43 (Fig. S9). However, compared to control iPSC-CMs (n=368) at day 30 post differentiation, a significant higher percentage of DCM iPSC-CMs (n=391) showed a punctate distribution of sarcomeric α-actinin over one fourth of the total cellular area (p=0.008) (Fig. 2A, 2B and Fig. S10, A to C). There were no significant differences in cell size between control and DCM iPSC-CMs (Fig. 2C) at this stage. This phenotype was consistently observed in two different DCM iPSC lines each from the 4 DCM patients, suggesting a homogeneous correlation to the disease-associating R173W mutation. Sarcomeric α-actinin is an excellent marker for sarcomeric integrity and degeneration and was used for evaluation of sarcomeric organizations in heart tissues from human patients with DCM (25). These results therefore suggest that, compared to the controls, an increased number of DCM iPSC-CMs had a more disturbed sarcomeric organization at this stage. Notably, CMs clusters always showed a much less disturbed sarcomeric pattern (Fig. S10, D and E). The majority of CMs with punctate sarcomeric α-actinin distribution were single cells or cells at the very edge of CMs clusters (Fig. S10, D and E), suggesting a higher tendency for single TNNT2 R173W DCM iPSC-CMs to malfunction in maintaining sarcomere integrity. To further assess the myofibrillar organization in detail, we performed transmission electron microscopy (TEM) on both control and DCM iPSC-CMs at day 30 post differentiation. Well organized myofibrils with aligned Z-lines and recognizable A-bands and I bands were found in both control (n=11) and DCM iPSC-CMs (n=12) (Fig. 2D and Fig. S10F), although mitochondria and sarcoplasmic reticulum were still immature in both groups at this stage (Fig. S10, G and H). However, compared to controls, DCM iPSC-CMs exhibited an increased variability in the degree of sarcomeric organization, with a higher number of less well-aligned Z-lines and scattered patterns of condensed Z-bodies (Fig. 2D and Fig. S10F). Overall, these results are consistent

with the sarcomeric α-actinin immunostaining in DCM CMs shown in Fig. 2A and Fig. S10, A to C.

TNNT2 R173W DCM iPSC-CMs are more susceptible to chronotropic and mechanical stress

Positive inotropic stress can induce DCM phenotype in transgenic mouse models of DCM (26–27) and aggravate the disease in clinical patients (28). We next examined whether treatment with positive inotropic reagent, such as β-adrenergic agonists, can expedite the phenotypic response of DCM iPSC-CMs. Indeed, we found that 10 μM norepinephrine (NE) treatment induced an initial positive chronotropic effect that later became negative, eventually leading to failure of spontaneous contraction in DCM iPSC-derived beating EBs (n=14) as reflected by MEA recording. By contrast, the control iPSC-derived beating EBs (n=14) exhibited prolonged positive chronotropic activity (Fig. 3A). One week of 10 μM NE treatment *in vitro* markedly increased the number of CMs with punctate sarcomeric α-actinin distribution from DCM iPSC clones, with almost 80–90% of the DCM iPSC-CMs found to have the disorganized sarcomeric pattern (Fig. 3B, 3C, and Fig. S11, A to E). A few single DCM iPSC-CMs showed complete degeneration of myofilaments after prolonged NE treatment (Fig. 3B and Fig. S11A), which was not observed in control iPSC-CMs. TEM analyses indicated that, compared to controls (n=6), NE-treated DCM iPSC-CMs (n=7) exhibited a more severe scattered distribution of Z-bodies (Fig. 3D and Fig. S11F), which was consistent with the markedly increased heterogeneous pattern of sarcomeric α-actinin staining after NE treatment. Tracking with video imaging of individual beating clusters of both control and DCM iPSC-CMs treated with 10 μM NE over time showed distinct outcomes. Decreased inotropic and chronotropic activities were often observed in the DCM iPSC-CMs (Fig. 3E, 3F, and Videos S8 to S15). These results suggest that DCM iPSC-CMs are more susceptible to the stress of β-adrenergic stimulation.

Biomechanical stress generated by pressure or volume overload resulted from hypertension or myocardial injury often induce DCM and heart failure, and tends to aggravate the disease (29). We next examined the effect of mechanical stress on iPSC-CMs by cyclic stretch. Prolonged stretching led to significant thickening and loss of obvious striation of the myofibrils in both control and DCM iPSC-CMs (Fig. S12, A and B). Mechanical strain also significantly increased the number of cells with relative disorganized sarcomeric pattern in both control and DCM iPSC-CMs. However, compared to controls, an increased heterogeneity in sarcomeric pattern was observed in DCM iPSC-CMs (Fig. S12C). These results suggest that DCM iPSC-CMs are more susceptible to biomechanical stress.

TNNT2 R173W DCM iPSC-CMs exhibit altered Ca^{2+} handling

CM contraction starts from the electrical excitation of the myocytes, as reflected by the membrane action potentials (APs) (30). To investigate the possible underlying etiology, we assessed whether the DCM-associating R173W mutation in TNNT2 affects the electrical excitation of the CMs. We examined the electrical activities of the dissociated single beating iPSC-CMs by patch clamping. Three types of spontaneous APs (ventricular-like, atrial-like, and nodal-like) were observed in both control and DCM iPSC-CMs (Fig. 4A). DCM ventricular-like myocytes (n=17) exhibited normal APs that were comparable to control (n=18) (Fig. 4B). The average action potential duration at 90% repolarization (APD90) of the DCM iPSC-CMs was not significantly different from that seen in control iPSC-CMs (Fig. 4C). The average AP frequency, peak amplitude, and resting potential were also very similar between the 2 groups (Fig. 4D to 4F). These results indicate that the electrical activities of individual control and DCM iPSC-CMs were normal at baseline, consistent with the results obtained by MEA analysis of beating EBs.

To further investigate the underlying DCM disease mechanism, we measured the Ca^{2+} handling properties at the excitation-contraction coupling level by fluorescent Ca^{2+} imaging. DCM iPSC-CMs (n=40, 5 lines from 3 DCM patients, Table S3) exhibited rhythmic frequency and timing comparable to those of the control iPSC-CMs (n=87, 5 lines from 3 control individuals, Table S3) (Fig. 5A, 5B, 5C, 5E, and 5F). However, DCM iPSC-CMs exhibited significantly smaller $[Ca^{2+}]_i$ transient amplitudes compared to those of the control iPSC-CMs (p=0.002) (Fig. 5D), indicating the $[Ca^{2+}]_i$ available for each contraction of DCM iPSC-CMs was significantly lower. The smaller $[Ca^{2+}]_i$ transients of CMs were consistently observed in all examined DCM iPSC lines, suggesting weaker force production in DCM iPSC-CMs. To further analyze the Ca^{2+} handling properties of iPSC-CMs, both control and DCM iPSC-CMs were subjected to caffeine treatment to induce the Ca^{2+} release from the sarcoplasmic reticulum (SR) through ryanodine receptor (RyR) Ca^{2+} channels (Fig. 5, G–J). Compared to controls, DCM iPSC-CMs exhibited relatively smaller amplitudes, prolonged time to peak, and delayed decay time (Fig. 5, H–J), indicating that DCM iPSC-CMs have a relatively lower SR Ca^{2+} storage and altered function of Ca^{2+} related molecules such as SR Ca^{2+} release channels and Ca^{2+} pumps in the plasma and SR membranes.

TNNT2 R173W DCM iPSC-CMs exhibit compromised contractility

Deficiency in contractile force production is one of the most important mechanisms responsible for inducing DCM and heart failure (4). To investigate this further, we next measured the contraction force of iPSC-CMs using atomic force microscopy (AFM), which has been used to measure contraction of cultured chicken embryonic CMs (31). The AFM allowed us to probe the contractile properties at the single cell level (Fig. S13 and Video S16). Compared to single control iPSC-CMs (n=13), the DCM iPSC-CMs (n=17) showed similar beat frequency and duration (Fig. S14) but significantly weaker contraction forces (Fig. 6A, 6B, and Table S5). There was no correlation between the cell size and contraction force for each single cell measured by AFM (Fig. S15).

Serca2a over-expression enhanced contractility in TNNT2 R173W DCM iPSC-CMs

Previous studies have shown that Serca2a over-expression, a treatment investigated in a pre-clinical trial (32), mobilized intracellular Ca^{2+} and restored contractility of cardiomyocytes in failing human hearts and improved failing heart functions in animal models (33–35). Given our results showing smaller Ca^{2+} transients and compromised contractility in the DCM iPSC-CMs, we hypothesized that over-expression of Serca2a may rescue the phenotypes of DCM iPSC-CMs. Transduction of DCM iPSC-CMs with adenoviruses carrying Serca2a co-expressing GFP (Ad.Seca2a) (see **Material and Methods** section) at a multiplicity of infection (MOI) of 100 led to over-expression of Serca2a in these cells (Fig. 6C). Co-expression of GFP along with Serca2a allowed us to recognize the individual transduced cells and measure their contractile forces by AFM (Fig. 6D and Videos S17 to S20). After 48 hours of transduction, over-expression of Serca2a (n=12) restored the contractile force of single DCM iPSC-CMs to a level similar to that seen in control iPSC-CMs (Fig. 6A, 6B, and Table S5). Ca^{2+} imaging using the red fluorescent Ca^{2+} indicator Rhod-2 AM (Fig. S16) indicated that DCM iPSC-CMs transduced with Ad.Serca2a co-expressing GFP (n=22) had significantly increased global $[Ca^{2+}]_i$ transients compared to cells transduced with Ad.GFP only (n=14) (Fig. 6, E and F) (p=0.04), which is consistent with the restored force production. Although Rhod-2 Ca^{2+} dye is not ideal to quantify cytoplasmic Ca^{2+} level (since it is difficult to calibrate its level using the indicator in live cells), the kinetics of Ca^{2+} transients and sarcomeric organization in Serca2a-transduced DCM iPSC-CMs was not significantly changed (Fig. 6, G and H). On the other hand, over-expression of Serca2a in control iPSC-CMs failed to produce a statistically significant increase in contractility (Fig. S17), likely because the endogenous amount and function of SERCA were already at a relatively high level in control cells. Altogether, these results

demonstrate that over-expression of Serca2a increased the $[Ca^{2+}]_i$ transients and contraction force of DCM iPSC-CMs and improved their function to some extent.

Gene expression profiling of DCM iPSC-CMs following adenoviral Serca2a delivery

Although Serca2a gene therapy is now in clinical trial, the overall mechanism of individual CM cellular response after Serca2a gene therapy has not been extensively studied previously (36). Hence we set out to investigate the mechanisms by which Serca2a delivery might repair defects in DCM iPSC-CMs. Gene expression profiling of Serca2a-transduced control and DCM iPSC-CMs showed different sets of genes had greater than 2-fold expression changes, indicating different responses to Serca2a over-expression (Table S6 and S7). There were 191 genes (65 upregulated and 126 downregulated) with greater than 2 fold expression changes in DCM iPSC-CMs over-expressed with Serca2a that were rescued to an expression level similar to those in control iPSC-CMs (Fig. S18A). Enriched pathways analysis indicated that several previously known pathways, such as Ca^{2+} signaling, protein kinase A signaling, and G-protein coupled receptor signaling, are significantly involved in rescuing the DCM phenotype by Serca2a over-expression (37–38). Interestingly, several pathways not previously linked to DCM, including factors promoting cardiogenesis, integrin and cytoskeletal signaling, and ubiquitination pathway, were also found to participate in rescuing the DCM CM function (Fig. S18B and Table S8).

β-adrenergic blocker improved sarcomeric organization of DCM iPSC-CMs

Clinical studies have shown that metoprolol, a β1-selective β-adrenergic blocker, has a beneficial effect on the clinical symptoms and hemodynamic status of DCM patients (39–40). We thus tested whether *in vitro* metoprolol treatment has a beneficial effect on the TNNT2 R173 DCM iPSC-CMs as well. We found that 10 μM metoprolol treatment for one week significantly decreased the number of single DCM iPSC-CMs with disorganized sarcomericα-actinin staining (Fig. S19A). Although not statistically significant, metoprolol treatment on DCM iPSC-CMs resulted in a relatively reduced chronotropic effect and increased global Ca^{2+} transients on DCM iPSC-CMs (Fig. S19, B to D). Metoprolol treatment also significantly prevented aggravation of the DCM iPSC-CMs that is induced by NE treatment (Fig. S19E). No significant effect on sarcomeric α-actinin distribution in control iPSC-CMs treated with metoprolol was observed (Fig. S19F). These results suggest that blockade ofβ-adrenergic pathway helped DCM iPSC-CMs resist mechanical deterioration and improved their myofilament organization.

DISCUSSION

We have generated patient-specific iPSCs from a DCM family carrying a single point mutation R173W in the sarcomeric protein cTnT and derived CMs from these iPSCs. This has allowed us to generate, for the first time, a large number of human DCM-specific iPSC-CMs and to analyze their functional properties, explore the potential underlying etiology, and test effective therapies. Although the TNNT2 R173W mutation does not seem to affect other cells from cardiovascular lineage (Fig. S20), we observed significant phenotypic differences between the control and DCM iPSC-CMs.

Increased heterogeneity in sarcomeric organization in TNNT2 R173W DCM iPSC-CMs

In this study, a higher tendency of disturbance in sarcomeric organization was observed in DCM iPSC-CMs. An increased number of DCM iPSC-CMs exhibited punctate sarcomericα-actinin staining in immunocytochemistry and a more scattered distribution pattern of Z-bodies in transmission electron microscopy. Notably, this phenotype was more frequently observed in single cells or cells at the very edges of a cluster than in cells within the inner side of a cluster. The heterogeneous presentation of sarcomeric organization in

iPSC-CMs could be explained by the following hypotheses. First, individual CMs and CM clusters have different architectural matrices and physical properties in tolerating mechanical forces generated by spontaneous contractions, leading to heterogeneous sarcomeric organization. As in the analogy to breaking chopsticks, a bundle of chopsticks will tolerate much stronger breaking force than just one. Second, CMs seeded on culture dishes confront different environmental factors, such as the topology of attaching surfaces and paracrine factors from surrounding cells, leading to heterogeneous myofilament organization. It is actually not unusual to observe heterogeneous sarcomeric organization in cultured rat neonatal CMs as shown by previous studies (41–42). The increased heterogeneous presentation of sarcomeric organization in DCM iPSC-CMs could be explained by their higher susceptibility to stress. Indeed, both β-agonist stimulation and cyclic stretch markedly increased the heterogeneity of sarcomeric organization in DCM iPSC-CMs, indicating they were more susceptible to positive inotropic stress.

Overall, our data are consistent to some extent with previous studies showing that muscle LIM protein (MLP)-deficient mice neonatal DCM CMs and zebrafish embryonic DCM heart tissues with mutations in nexilin were more susceptible to mechanical stress (43–44). These results suggest that DCM iPSC-CMs are less capable of maintaining their sarcomeric integrity compared to control iPSC-CMs, and more susceptible to positive inotropic and chronotropic stress.

Abnormal Ca^{2+} handling and weaker contractility in TNNT2 R173W DCM iPSC-CMs

While the baseline electrophysiological activities of the DCM iPSC-CMs were not significantly different from those of the controls, abnormal Ca^{2+} transients were found in the DCM iPSC-CMs. These results suggest that DCM iPSC-CMs have impaired Ca^{2+} handling associated with a lower contractility. Gene expression profiling using microarray analysis also indicates that DCM iPSC-CMs express a lower level of Ca^{2+}-related key molecules (CASQ, TMEM38, NFAT, and NECAB) which is consistent with the compromised Ca^{2+} handling properties observed on Ca^{2+} imaging. Finally, AFM analyses indicate that individual DCM iPSC-CMs manifest decreased contractile force compared to controls, which is consistent with the smaller $[Ca^{2+}]_i$ transients observed. Interestingly, previous studies have also shown altered Ca^{2+} handing in CMs isolated from human patients with heart failure (45). These CMs represent a very late stage of the disease, and it is still not clear whether the altered Ca^{2+} handing is the primary factor that contributes to the disease or merely a secondary consequence of the disease progression. Our current model of DCM using iPSC-CMs represents a very early stage of heart development, showing that abnormalities in Ca^{2+} handing can occur at very early stage.

Possible contribution of R173W cTnT mutation to the phenotypes observed in DCM iPSC-CMs

Although there is no biochemical data showing how the particular cTnT R173W mutation impact the Ca^{2+} sensitivity or ATPase activity of the myofibers in the current literature, a major outcome of most of the cTnT mutations affecting DCM is a decreased Ca^{2+} sensitivity in the myofilaments (9–10,13–14). Decreased Ca^{2+} sensitivity usually suggests a decreased contractility in the myofibers at the physiological cytosolic Ca^{2+} concentration. Indeed, our AFM data indicated that the R173W cTnT DCM iPSC-CMs had decreased contractility compared to controls. It is likely that decreased contraction attenuates maturation of the DCM iPSC-CMs as well as the mechanical stretch-induced gene expression of molecules associated with myofilament and Ca^{2+} handling in DCM cells (Fig. S21), resulting in an increased heterogeneity in sarcomeric organization under inotropic and mechanical stress. Altered Ca^{2+} handling also possibly induced a reduction in Ca^{2+} transients under the condition without *in vivo* remodeling, which further decreased the contractility of DCM

iPSC-CMs *in vitro.* This could form a negative cycle which eventually compromises the overall CMs function. Although a direct relationship between the R173W cTnT mutation and the abnormal Ca^{2+} handling has not been well-established, the defects in gene expression in our study suggest that the contractility and Ca^{2+} handling phenotypes were secondary consequences of the R173W mutation in DCM iPSC-CMs. Further biochemical and molecular studies are required in the future to understand the disease progression and the overall DCM mechanisms induced by the R173W mutation in the cTnT gene.

Beneficial effect of metoprolol pharmacologic treatment and Serca2a gene delivery

We have demonstrated that prolonged treatment of β-blocker metoprolol had a beneficial effect on the DCM iPSC-CMs' abnormal sarcomeric phenotype by decreasing the number of single CMs with abnormal sarcomeric α-actinin staining. Metoprolol treatment led to a relatively negative chronotropic effect and an improved global Ca^{2+} transient on DCM iPSC-CMs. These results are consistent with a previous study showing that metoprolol treatment on cultured neonatal rat CMs induced both negative chronotropic and positive inotropic effect on fast beating cells (46). These results also indicate that metoprolol can reduce the number of contraction in a given time, possibly reflecting an improved contraction force; they may represent some of the beneficial factors contributing to the protective effects on DCM iPSC-CMs. In addition, metoprolol treatment on cultured neonatal rat CMs have been shown to upregulate protein levels of cardiac gap junction channels (47), allowing a better connection and communication between cells. Altogether, these may exert beneficial effects on the DCM iPSC-CMs observed in our study.

We have also shown in this study that over-expression with Serca2a, a novel gene therapy treatment for heart failure currently in clinical trials (48), can significantly improve the contractile function of DCM iPSC-CMs. Delivery of exogenous Serca2a could prevent the possible negative cascades induced by the R173W mutation in cTnT (Fig. S21). It also overcame the phenotype of lower SR Ca^{2+} storage and contractility in DCM iPSC-CMs, thus rescuing the compromised contractility. Gene expression profiling further identified several novel pathways that are involved in Serca2a rescue, including ubiquitination and integrin signaling pathways. These results could also help guide further investigations of other molecular mechanisms underlying DCM and in finding potential targets to treat DCM in the future.

In summary, our data indicate that the TNNT2 R173W mutation caused impairment in myofilament regulation, Ca^{2+} handling, and force production of individual CMs, which might be the primary reason for the eventual appearance of the DCM clinical phenotype in patients. Despite some limitations in the current iPSC-CM platform (e.g., CM immaturity and lack of an *in vivo* environment for possible disease remodeling), our overall findings demonstrate that the iPSC platforms are useful to investigate disease mechanisms at an early stage of genetic diseases and to discover novel therapeutic targets. Patient-specific human iPSC-CMs model of DCM could be an important complement to the biochemical and mouse DCM models to help us understand the complex etiology and disease mechanisms. In the future, we anticipate more studies will use this platform for exploring mechanisms and treatments of the different genetic mutations responsible for familial DCM as well as other hereditary cardiovascular disorders.

MATERIALS AND METHODS

Patient-specific iPSC derivation, culture, and characterization

All of the protocols for this study were approved by the Stanford University Human Subjects Research Institutional Review Board. Generation of patient-specific iPSC lines were performed as previously described (49).

Cardiac differentiation of human ESCs and iPSCs

Differentiation into the cardiac lineage was performed using the protocol described by Yang *et al.* (24). Detailed procedure is described in the Supplementary Methods.

Ca^{2+} imaging

Dissociated iPSC-CMs were seeded in gelatin-coated 4-well LAB-TEK II chambers (Nalge Nunc International) and were loaded with 5 μM Fluo-4 AM or 2 μM Rhod-2 AM (for cells expressing GFP) and 0.02 % Pluronic F-127 (all from Molecular Probes) in the Tyrodes solution (140 mM NaCl, 5.4 mM KCl, 1 mM $MgCl_2$, 10 mM glucose, 1.8 mM $CaCl_2$, and 10 mM HEPES pH 7.4 with NaOH at 25°C) for 15 min at 37°C. Cells were then washed three times with the Tyrodes solution. Ca^{2+} imaging was conducted with a confocal microscope (Carl Zeiss, LSM 510 Meta) with a 63x lens (NA=1.4) using Zen software. Spontaneous Ca^{2+} transients were acquired at room temperature using line scan mode at a sampling rate of 1.92 ms/line. A total of 10,000 lines were acquired for 19.2 s recoding. For Measurement of caffeine-evoked Ca^{2+} release, caffeine (20 mM) in Ca^{2+} free solution (Tyrodes solution containing 5 mM EGTA instead of $CaCl_2$) was used to evoke SR/ER Ca^{2+} transients in iPSC-CMs.

Atomic force microscopy (AFM)

iPSC-CMs were seeded on glass bottom petri dishes before each experiment, and switched from culture media to warm Tyrode's solution. Cells were maintained at 36°C for the entire experiment. Beating cells were interrogated by AFM (MFP-3D Bio, Asylum Research) using a silicon nitride cantilever (spring constants ~0.04 N/m, BudgetSensors). To measure forces, cells were gently contacted by the cantilever tip with 100 pN of force, with a typical cellular indentation of around 100–200 nm, with the cantilever tip remained in the position without Z-piezo feedback for multiple sequential two minute intervals while deflection data were collected at a sample rate of 2 kHz. Typical noise during these measurements was around 20 pN. Deflection data were converted to force by multiplying by the spring constant. Typically, 100–400 beats were collected for each single cell, and statistics were calculated for the forces, intervals between beats, and duration of each contraction. Forces across cells were compared using two tailed Student's t-test.

Adenovirus transduction of iPSC-CMs

First-generation type 5 recombinant adenoviruses carrying cytomegalovirus (CMV) promoter driving Serca2a plus a separate CMV promoter driving GFP (Ad.Serca2a) and adenoviruses carrying CMV promoter driving GFP only (Ad.GFP) as control were used (35). Dissociated iPSC-CMs were transduced at MOI 100 overnight and then refreshed with culture medium (DMEM supplemented with 10% FBS). Cells were used for subsequent experiments 48 hours after transduction.

Statistical analysis

Data were analyzed using either Excel or R. Statistical differences among two groups were tested using two tailed Student's t-tests. Statistical differences among more than two groups

were analyzed using one-way ANOVA tests followed by Tukey's Multiple Comparison Test. Significant differences were determined when p value is less than 0.05.

Supplementary Material

Refer to Web version on PubMed Central for supplementary material.

Acknowledgments

We thank Dr. Shinji Komazaki at the Department of Anatomy, Saitama Medical University for his advice on transmission electron microscopic analyses, and Dr. Beth Pruitt at the Department of Biochemistry, Stanford University for her help with stretch experiments.

Funding: Supported by NIH New Innovator Award DP2OD004437, RC1 AG036142, R33 HL093172, CIRM RB3-05129 (JCW), RC1 HL100490 (MTL, JCW), U01 HL099776 (RCR), P01GM099130 (MPS), Swiss National Science Foundation PBBEP3_129803 (VSF), AHA WSA Postdoctoral Fellowship 10POST3730079 (SH), AHA WSA Postdoctoral Fellowship 10POST3870063 (MY), and the Oak Foundation Cardiovascular Fellowship (NS).

References

1. Maron BJ, Towbin JA, Thiene G, Antzelevitch C, Corrado D, Arnett D, Moss AJ, Seidman CE, Young JB. Contemporary definitions and classification of the cardiomyopathies: an American Heart Association Scientific Statement from the Council on Clinical Cardiology, Heart Failure and Transplantation Committee; Quality of Care and Outcomes Research and Functional Genomics and Translational Biology Interdisciplinary Working Groups; and Council on Epidemiology and Prevention. Circulation. 2006; 113:1807–1816. [PubMed: 16567565]
2. Harmon WE, McDonald RA, Reyes JD, Bridges ND, Sweet SC, Sommers CM, Guidinger MK. Pediatric transplantation, 1994–2003. Am J Transplant. 2005; 5:887–903. [PubMed: 15760416]
3. Roura S, Bayes-Genis A. Vascular dysfunction in idiopathic dilated cardiomyopathy. Nat Rev Cardiol. 2009; 6:590–598. [PubMed: 19636323]
4. Morita H, Seidman J, Seidman CE. Genetic causes of human heart failure. J Clin Invest. 2005; 115:518–526. [PubMed: 15765133]
5. Burkett EL, Hershberger RE. Clinical and genetic issues in familial dilated cardiomyopathy. J Am Coll Cardiol. 2005; 45:969–981. [PubMed: 15808750]
6. Knoll R, Hoshijima M, Hoffman HM, Person V, Lorenzen-Schmidt I, Bang ML, Hayashi T, Shiga N, Yasukawa H, Schaper W, McKenna W, Yokoyama M, Schork NJ, Omens JH, McCulloch AD, Kimura A, Gregorio CC, Poller W, Schaper J, Schultheiss HP, Chien KR. The cardiac mechanical stretch sensor machinery involves a Z disc complex that is defective in a subset of human dilated cardiomyopathy. Cell. 2002; 111:943–955. [PubMed: 12507422]
7. Sehnert AJ, Huq A, Weinstein BM, Walker C, Fishman M, Stainier DY. Cardiac troponin T is essential in sarcomere assembly and cardiac contractility. Nat Genet. 2002; 31:106–110. [PubMed: 11967535]
8. Willott RH, Gomes AV, Chang AN, Parvatiyar MS, Pinto JR, Potter JD. Mutations in Troponin that cause HCM, DCM AND RCM: what can we learn about thin filament function? J Mol Cell Cardiol. 2010; 48:882–892. [PubMed: 19914256]
9. Hershberger RE, Pinto JR, Parks SB, Kushner JD, Li D, Ludwigsen S, Cowan J, Morales A, Parvatiyar MS, Potter JD. Clinical and functional characterization of TNNT2 mutations identified in patients with dilated cardiomyopathy. Circ Cardiovasc Genet. 2009; 2:306–313. [PubMed: 20031601]
10. Morimoto S. Molecular pathogenic mechanisms of cardiomyopathies caused by mutations in cardiac troponin T. Adv Exp Med Biol. 2007; 592:227–239. [PubMed: 17278368]
11. Ahmad F, Banerjee SK, Lage ML, Huang XN, Smith SH, Saba S, Rager J, Conner DA, Janczewski AM, Tobita K, Tinney JP, Moskowitz IP, Perez-Atayde AR, Keller BB, Mathier MA, Shroff SG, Seidman CE, Seidman JG. The role of cardiac troponin T quantity and function in cardiac development and dilated cardiomyopathy. PLoS One. 2008; 3:e2642. [PubMed: 18612386]

12. Lombardi R, Bell A, Senthil V, Sidhu J, Noseda M, Roberts R, Marian AJ. Differential interactions of thin filament proteins in two cardiac troponin T mouse models of hypertrophic and dilated cardiomyopathies. Cardiovasc Res. 2008; 79:109–117. [PubMed: 18349139]

13. Lu QW, Morimoto S, Harada K, Du CK, Takahashi-Yanaga F, Miwa Y, Sasaguri T, Ohtsuki I. Cardiac troponin T mutation R141W found in dilated cardiomyopathy stabilizes the troponin T-tropomyosin interaction and causes a Ca2+ desensitization. J Mol Cell Cardiol. 2003; 35:1421–1427. [PubMed: 14654368]

14. Morimoto S, Lu QW, Harada K, Takahashi-Yanaga F, Minakami R, Ohta M, Sasaguri T, Ohtsuki I. Ca(2+)-desensitizing effect of a deletion mutation Delta K210 in cardiac troponin T that causes familial dilated cardiomyopathy. Proc Natl Acad Sci U S A. 2002; 99:913–918. [PubMed: 11773635]

15. Yu J, Vodyanik MA, Smuga-Otto K, Antosiewicz-Bourget J, Frane JL, Tian S, Nie J, Jonsdottir GA, Ruotti V, Stewart R, Slukvin, Thomson JA. Induced pluripotent stem cell lines derived from human somatic cells. Science. 2007; 318:1917–1920. [PubMed: 18029452]

16. Takahashi K, Tanabe K, Ohnuki M, Narita M, Ichisaka T, Tomoda K, Yamanaka S. Induction of pluripotent stem cells from adult human fibroblasts by defined factors. Cell. 2007; 131:861–872. [PubMed: 18035408]

17. Zhang J, Wilson GF, Soerens AG, Koonce CH, Yu J, Palecek SP, Thomson JA, Kamp TJ. Functional cardiomyocytes derived from human induced pluripotent stem cells. Circ Res. 2009; 104:e30–41. [PubMed: 19213953]

18. Zwi L, Caspi O, Arbel G, Huber I, Gepstein A, Park IH, Gepstein L. Cardiomyocyte differentiation of human induced pluripotent stem cells. Circulation. 2009; 120:1513–1523. [PubMed: 19786631]

19. Carvajal-Vergara X, Sevilla A, D'Souza SL, Ang YS, Schaniel C, Lee DF, Yang L, Kaplan AD, Adler ED, Rozov R, Ge Y, Cohen N, Edelmann LJ, Chang B, Waghray A, Su J, Pardo S, Lichtenbelt KD, Tartaglia M, Gelb BD, Lemischka IR. Patient-specific induced pluripotent stem-cell-derived models of LEOPARD syndrome. Nature. 2010; 465:808–812. [PubMed: 20535210]

20. Moretti A, Bellin M, Welling A, Jung CB, Lam JT, Bott-Flugel L, Dorn T, Goedel A, Hohnke C, Hofmann F, Seyfarth M, Sinnecker D, Schomig A, Laugwitz KL. Patient-specific induced pluripotent stem-cell models for long-QT syndrome. N Engl J Med. 2010; 363:1397–1409. [PubMed: 20660394]

21. Itzhaki I, Maizels L, Huber I, Zwi-Dantsis L, Caspi O, Winterstern A, Feldman O, Gepstein A, Arbel G, Hammerman H, Boulos M, Gepstein L. Modelling the long QT syndrome with induced pluripotent stem cells. Nature. 2011; 471:225–229. [PubMed: 21240260]

22. Yazawa M, Hsueh B, Jia X, Pasca AM, Bernstein JA, Hallmayer J, Dolmetsch RE. Using induced pluripotent stem cells to investigate cardiac phenotypes in Timothy syndrome. Nature. 2011; 471:230–234. [PubMed: 21307850]

23. Van Acker H, De Sutter J, Vandekerckhove K, de Ravel TJ, Verhaaren H, De Backer J. Dilated cardiomyopathy caused by a novel TNNT2 mutation-added value of genetic testing in the correct identification of affected subjects. Int J Cardiol. 2010; 144:307–309. [PubMed: 19324435]

24. Yang L, Soonpaa MH, Adler ED, Roepke TK, Kattman SJ, Kennedy M, Henckaerts E, Bonham K, Abbott GW, Linden RM, Field LJ, Keller GM. Human cardiovascular progenitor cells develop from a KDR+ embryonic-stem-cell-derived population. Nature. 2008; 453:524–528. [PubMed: 18432194]

25. Hein S, Block T, Zimmermann R, Kostin S, Scheffold T, Kubin T, Klovekorn WP, Schaper J. Deposition of nonsarcomeric alpha-actinin in cardiomyocytes from patients with dilated cardiomyopathy or chronic pressure overload. Exp Clin Cardiol. 2009; 14:e68–75. [PubMed: 20098571]

26. Gramlich M, Michely B, Krohne C, Heuser A, Erdmann B, Klaassen S, Hudson B, Magarin M, Kirchner F, Todiras M, Granzier H, Labeit S, Thierfelder L, Gerull B. Stress-induced dilated cardiomyopathy in a knock-in mouse model mimicking human titin-based disease. J Mol Cell Cardiol. 2009; 47:352–358. [PubMed: 19406126]

27. Chandar S, Yeo LS, Leimena C, Tan JC, Xiao XH, Nikolova-Krstevski V, Yasuoka Y, Gardiner-Garden M, Wu J, Kesteven S, Karlsdotter L, Natarajan S, Carlton A, Rainer S, Feneley MP, Fatkin D. Effects of mechanical stress and carvedilol in lamin A/C-deficient dilated cardiomyopathy. Circ Res. 2010; 106:573–582. [PubMed: 20019332]

28. Borow KM, Lang RM, Neumann A, Carroll JD, Rajfer SI. Physiologic mechanisms governing hemodynamic responses to positive inotropic therapy in patients with dilated cardiomyopathy. Circulation. 1988; 77:625–637. [PubMed: 3342493]
29. Chien KR. Stress pathways and heart failure. Cell. 1999; 98:555–558. [PubMed: 10490095]
30. Bers DM. Cardiac excitation-contraction coupling. Nature. 2002; 415:198–205. [PubMed: 11805843]
31. Domke J, Parak WJ, George M, Gaub HE, Radmacher M. Mapping the mechanical pulse of single cardiomyocytes with the atomic force microscope. Eur Biophys J. 1999; 28:179–186. [PubMed: 10192933]
32. Hajjar RJ, Zsebo K, Deckelbaum L, Thompson C, Rudy J, Yaroshinsky A, Ly H, Kawase Y, Wagner K, Borow K, Jaski B, London B, Greenberg B, Pauly DF, Patten R, Starling R, Mancini D, Jessup M. Design of a phase 1/2 trial of intracoronary administration of AAV1/SERCA2a in patients with heart failure. J Card Fail. 2008; 14:355–367. [PubMed: 18514926]
33. Miyamoto MI, del Monte F, Schmidt U, DiSalvo TS, Kang ZB, Matsui T, Guerrero JL, Gwathmey JK, Rosenzweig A, Hajjar RJ. Adenoviral gene transfer of SERCA2a improves left-ventricular function in aortic-banded rats in transition to heart failure. Proc Natl Acad Sci U S A. 2000; 97:793–798. [PubMed: 10639159]
34. Kawase Y, Ly HQ, Prunier F, Lebeche D, Shi Y, Jin H, Hadri L, Yoneyama R, Hoshino K, Takewa Y, Sakata S, Peluso R, Zsebo K, Gwathmey JK, Tardif JC, Tanguay JF, Hajjar RJ. Reversal of cardiac dysfunction after long-term expression of SERCA2a by gene transfer in a pre-clinical model of heart failure. J Am Coll Cardiol. 2008; 51:1112–1119. [PubMed: 18342232]
35. del Monte F, Harding SE, Schmidt U, Matsui T, Kang ZB, Dec GW, Gwathmey JK, Rosenzweig A, Hajjar RJ. Restoration of contractile function in isolated cardiomyocytes from failing human hearts by gene transfer of SERCA2a. Circulation. 1999; 100:2308–2311. [PubMed: 10587333]
36. Jessup M, Greenberg B, Mancini D, Cappola T, Pauly DF, Jaski B, Yaroshinsky A, Zsebo KM, Dittrich H, Hajjar RJ. Calcium Upregulation by Percutaneous Administration of Gene Therapy in Cardiac Disease (CUPID): A Phase 2 Trial of Intracoronary Gene Therapy of Sarcoplasmic Reticulum Ca2+-ATPase in Patients With Advanced Heart Failure. Circulation. 2011; 124:304–313. [PubMed: 21709064]
37. Lipskaia L, Chemaly ER, Hadri L, Lompre AM, Hajjar RJ. Sarcoplasmic reticulum Ca(2+) ATPase as a therapeutic target for heart failure. Expert Opin Biol Ther. 2010; 10:29–41. [PubMed: 20078230]
38. Tada M, Toyofuku T. SR Ca(2+)-ATPase/phospholamban in cardiomyocyte function. J Card Fail. 1996; 2:S77–85. [PubMed: 8951564]
39. Engelmeier RS, O'Connell JB, Walsh R, Rad N, Scanlon PJ, Gunnar RM. Improvement in symptoms and exercise tolerance by metoprolol in patients with dilated cardiomyopathy: a double-blind, randomized, placebo-controlled trial. Circulation. 1985; 72:536–546. [PubMed: 3893793]
40. Andersson B, Hamm C, Persson S, Wikstrom G, Sinagra G, Hjalmarson A, Waagstein F. Improved exercise hemodynamic status in dilated cardiomyopathy after beta-adrenergic blockade treatment. J Am Coll Cardiol. 1994; 23:1397–1404. [PubMed: 8176099]
41. Aoki H, Sadoshima J, Izumo S. Myosin light chain kinase mediates sarcomere organization during cardiac hypertrophy in vitro. Nat Med. 2000; 6:183–188. [PubMed: 10655107]
42. Yund EE, Hill JA, Keller RS. Hic-5 is required for fetal gene expression and cytoskeletal organization of neonatal cardiac myocytes. J Mol Cell Cardiol. 2009; 47:520–527. [PubMed: 19540241]
43. Hassel D, Dahme T, Erdmann J, Meder B, Huge A, Stoll M, Just S, Hess A, Ehlermann P, Weichenhan D, Grimmler M, Liptau H, Hetzer R, Regitz-Zagrosek V, Fischer C, Nurnberg P, Schunkert H, Katus HA, Rottbauer W. Nexilin mutations destabilize cardiac Z-disks and lead to dilated cardiomyopathy. Nat Med. 2009; 15:1281–1288. [PubMed: 19881492]
44. Arber S, Hunter JJ, Ross J Jr, Hongo M, Sansig G, Borg J, Perriard JC, Chien KR, Caroni P. MLP-deficient mice exhibit a disruption of cardiac cytoarchitectural organization, dilated cardiomyopathy, and heart failure. Cell. 1997; 88:393–403. [PubMed: 9039266]
45. Yano M, Ikeda Y, Matsuzaki M. Altered intracellular Ca2+ handling in heart failure. J Clin Invest. 2005; 115:556–564. [PubMed: 15765137]

46. Moins N, Renoux M, Boucher M, Gachon P. Paradoxal pharmacologic effects observed with beta-blocker agents on cardiac cells in culture. In Vitro Cell Dev Biol. 1991; 27A:147–150. [PubMed: 1673457]

47. Salameh A, Blanke K, Dhein S, Janousek J. Cardiac gap junction channels are upregulated by metoprolol: an unexpected effect of beta-blockers. Pharmacology. 2010; 85:203–210. [PubMed: 20215810]

48. Jessup M, Greenberg B, Mancini D, Cappola T, Pauly DF, Jaski B, Yaroshinsky A, Zsebo KM, Dittrich H, Hajjar RJ. Calcium Upregulation by Percutaneous Administration of Gene Therapy in Cardiac Disease (CUPID): a phase 2 trial of intracoronary gene therapy of sarcoplasmic reticulum Ca2+-ATPase in patients with advanced heart failure. Circulation. 2011; 124:304–313. [PubMed: 21709064]

49. Sun N, Panetta NJ, Gupta DM, Wilson KD, Lee A, Jia F, Hu S, Cherry AM, Robbins RC, Longaker MT, Wu JC. Feeder-free derivation of induced pluripotent stem cells from adult human adipose stem cells. Proc Natl Acad Sci U S A. 2009; 106:15720–15725. [PubMed: 19805220]

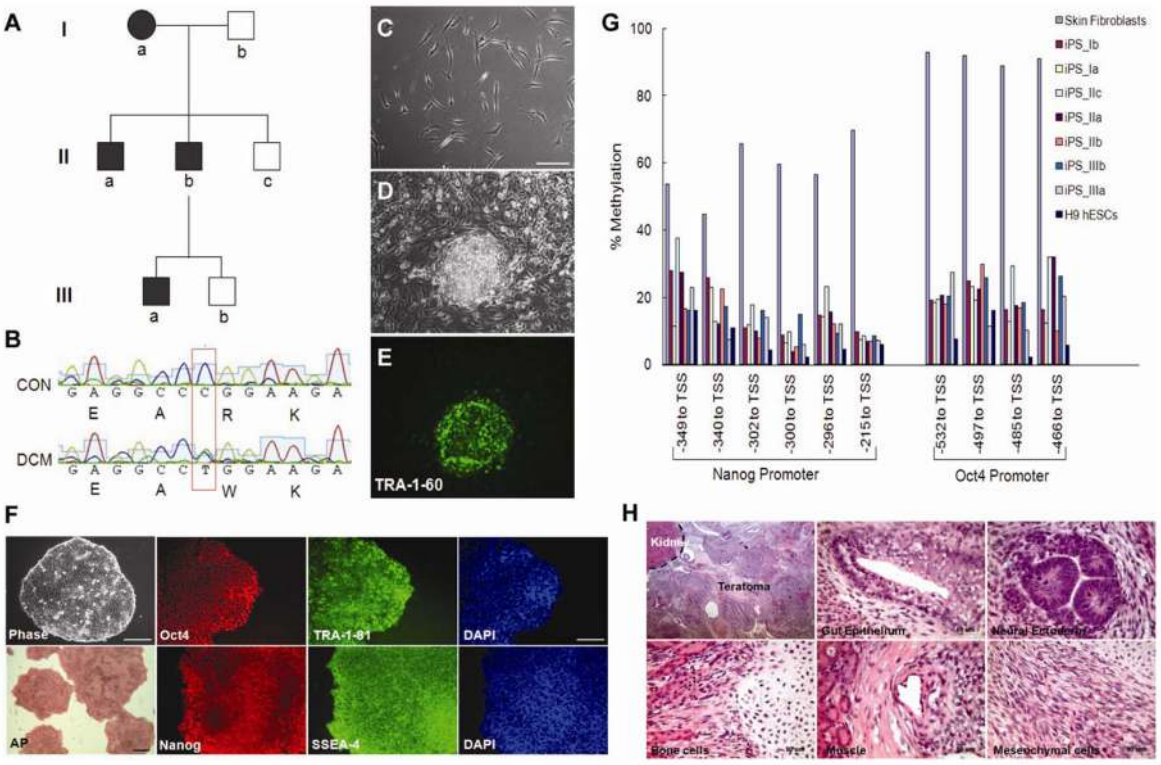

Figure 1. Generation of patient-specific DCM iPSCs

(A) Schematic pedigree of the DCM family recruited in this study. Filled squares (male) and circles (female) represent individuals carrying the specific heterozygous TNNT2 R173W mutation. **(B)** The R173W point mutation was confirmed to be present on exon 12 of the TNNT2 gene in the DCM patients by PCR and DNA sequencing. CON, control. **(C)** A representative image of the skin fibroblasts expanded from the skin biopsies. Representative images of an **(D)** ESC-like and **(E)** TRA-1-60 positive colony derived from reprogramming the skin fibroblasts with Yamanaka factors. **(F)** Immunofluorescence and alkaline phosphatase staining of the skin fibroblasts-derived iPSCs. **(G)** Quantitative bisulphite pyrosequencing analysis of the methylation status at the promoter regions of Oct4 and Nanog in the iPSCs. Both Nanog and Oct4 promoter regions were highly demethylated in the iPSCs derived. **(H)** Teratomas derived from the iPSCs injected into the kidney capsule of immunodeficient mice showing tissues of all three embryonic germ layers. Bars, 200 μm.

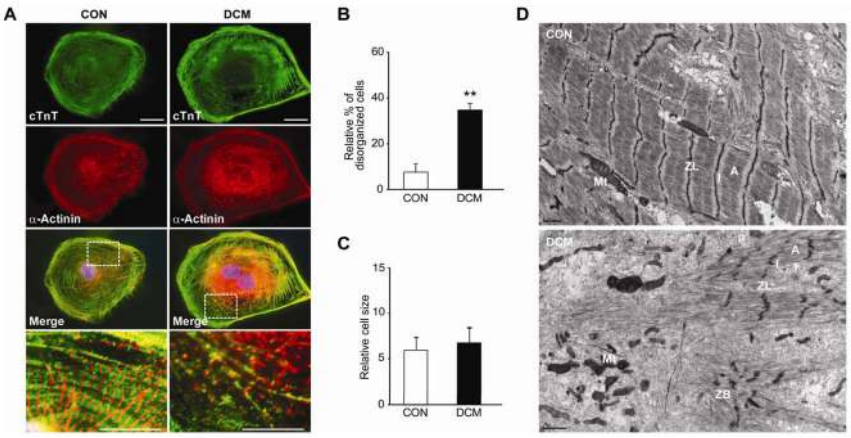

Figure 2. TNNT2 R173W DCM iPSC-CMs exhibited a significant higher number of cells with abnormal sarcomeric α-actinin distribution

(A) Immunostaining of sarcomeric α-actinin and cTnT at day 30 post differentiation. Single DCM iPSC-CMs exhibited punctate sarcomeric α-actinin distribution pattern suggesting a disorganized myofilament structure. Enlarged views of the boxed areas of the merged micrographs showing detailed α-actinin and cTnT staining pattern in the cells. Bars, 20 μm. **(B)** Compared to control iPSC-CMs (n=368), a significant higher percentage of DCM iPSC-CMs (n=391) showed punctate sarcomeric α-actinin staining pattern in greater than one fourth of the total cellular area (**p=0.008). **(C)** No significant difference was observed in cell size between control (n=36) and DCM iPSC-CMs (n=39). **(D)**, TEM images of myofibrillar organization in control and DCM iPSC-CMs. Compared to control CMs (n=11, 2 iPSC lines, one each from 2 individuals), myofibrils in DCM CMs (n=12, 2 iPSC lines, one each from 2 patients) exhibited an increased variability in the degree of organization. ZL, Z-line; ZB, Z-bodies; A, A-band; I, I-band; Mt, mitochondria. Extra TEM images of control and DCM CMs can be found in Fig. S10, F and G. Bars, 1μm.

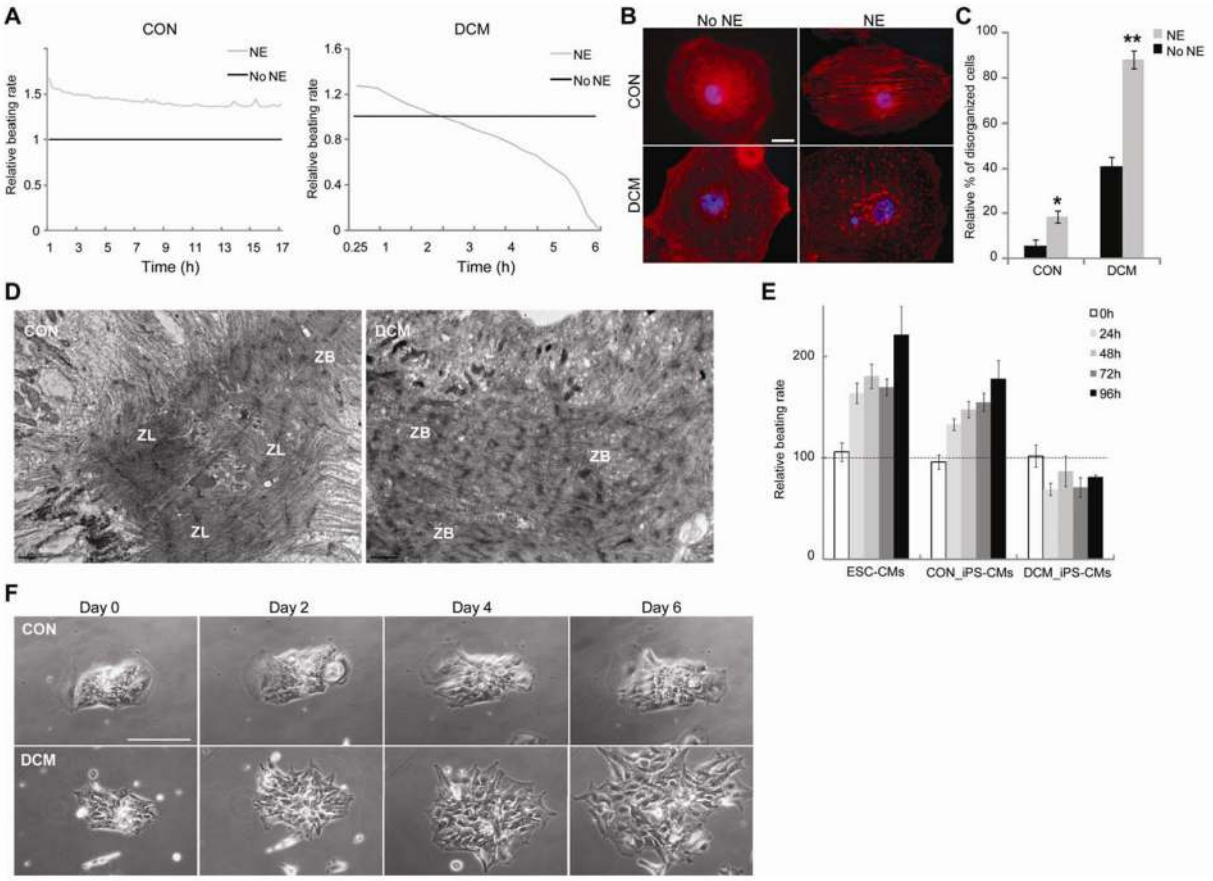

Figure 3. TNNT2 R173W DCM iPSC-CMs exhibited early failure after NE treatment

(A) A representative MEA assay recording chronotropic response of both control (n=14) and DCM (n=14) beating EBs overtime with 10 μM NE treatment. Electrical signals were recorded before and after NE treatment. Beating frequencies were normalized to the values before NE treatment. **(B)** Representative images of sarcomeric α-actinin immunostaining on single control and DCM iPSC-CMs after 7 days of NE treatment. Compared to the controls, long term NE treatment significantly aggravated sarcomeric organization of single DCM CMs. Bar, 20 μm. **(C)** Percentage of CMs with disorganized sarcomeric α-actinin staining pattern with (control, n=210; DCM, n=255) or without (control, n=261; DCM, n=277) NE treatment. NE treatment markedly increased the number of disorganized CMs in DCM group (**p<0.001), and had a less significant effect on control iPSC-CMs (*p=0.05). **(D)** TEM images of myofibrillar organization in control and DCM iPSC-CMs after NE treatment. Compared to control (n=6, 2 iPSC lines, one each from 2 individuals) CMs, myofibrils in DCM (n=7, 2 iPSC lines, one each from 2 patients) CMs exhibited an increased scattered distribution of Z-bodies. ZL, Z-line; ZB, Z-bodies. Extra TEM images of NE treated control and DCM CMs can be found in Fig. S11F. Bars, 1μm. **(E)** Relative beating frequencies of CM clusters (n = 10) over time after NE treatment by video imaging. Values are normalized to the beating frequencies of CM clusters at the same time points without NE treatment. Data are presented as mean±s.e.m. **(F)** Tracking morphological and contractility changes of iPSC-CMs overtime after NE treatment by video imaging. Bar, 200 μm. The respective videos were in Supplementary Information (Videos S8 to S15).

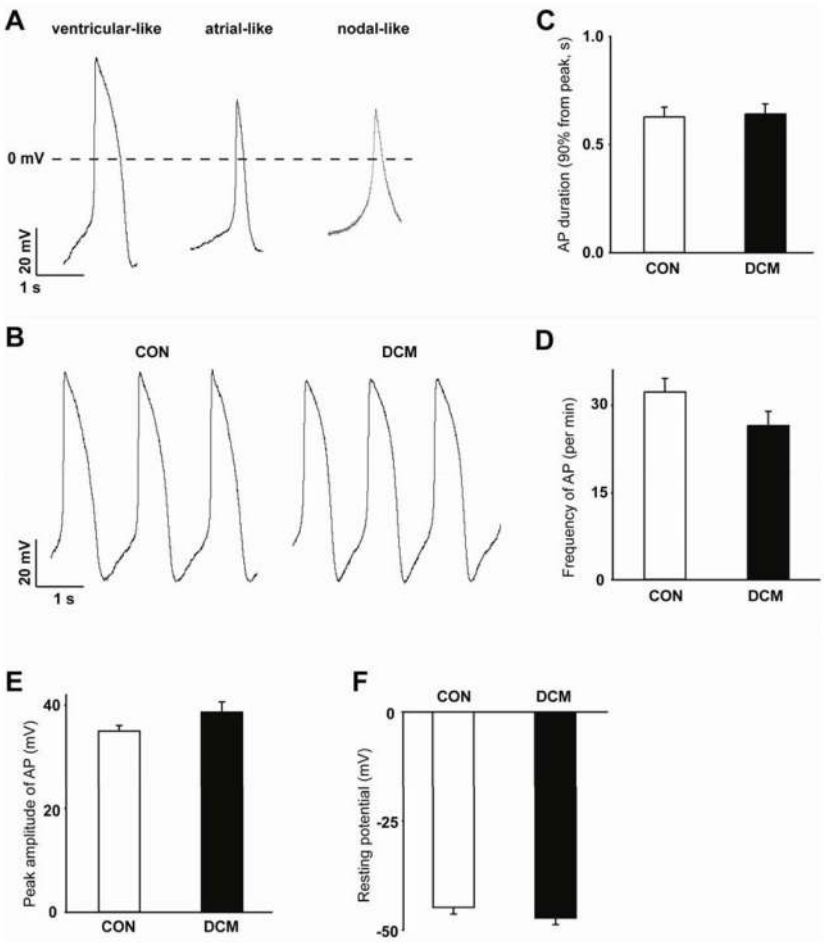

Figure 4. Electrophysiological features of iPSC-CMs measured by patch clamping

(A) Three types of spontaneous APs were observed in both control and DCM iPSC-CMs (left, ventricular-like; center, atrial-like; right, nodal-like). An estimated 70–80% cells were ventricular-like CMs, whereas the others were atrial- and/or nodal-like cells. There is no significant difference in cardiac cell fate between control and DCM iPSCs (data not shown). **(B)** Spontaneous APs in control and DCM ventricular-like myocytes using current-clamp recording. There was no significant difference in the AP durations **(C)**, frequency **(D),** the peak amplitude **(E)**, or in the resting membrane potential **(F)** between control and DCM cells at the time of measurements (day 19- day 25 post differentiation) (control, n=18; DCM, n=17). Statistical difference was tested using the two tailed Student's T-test.

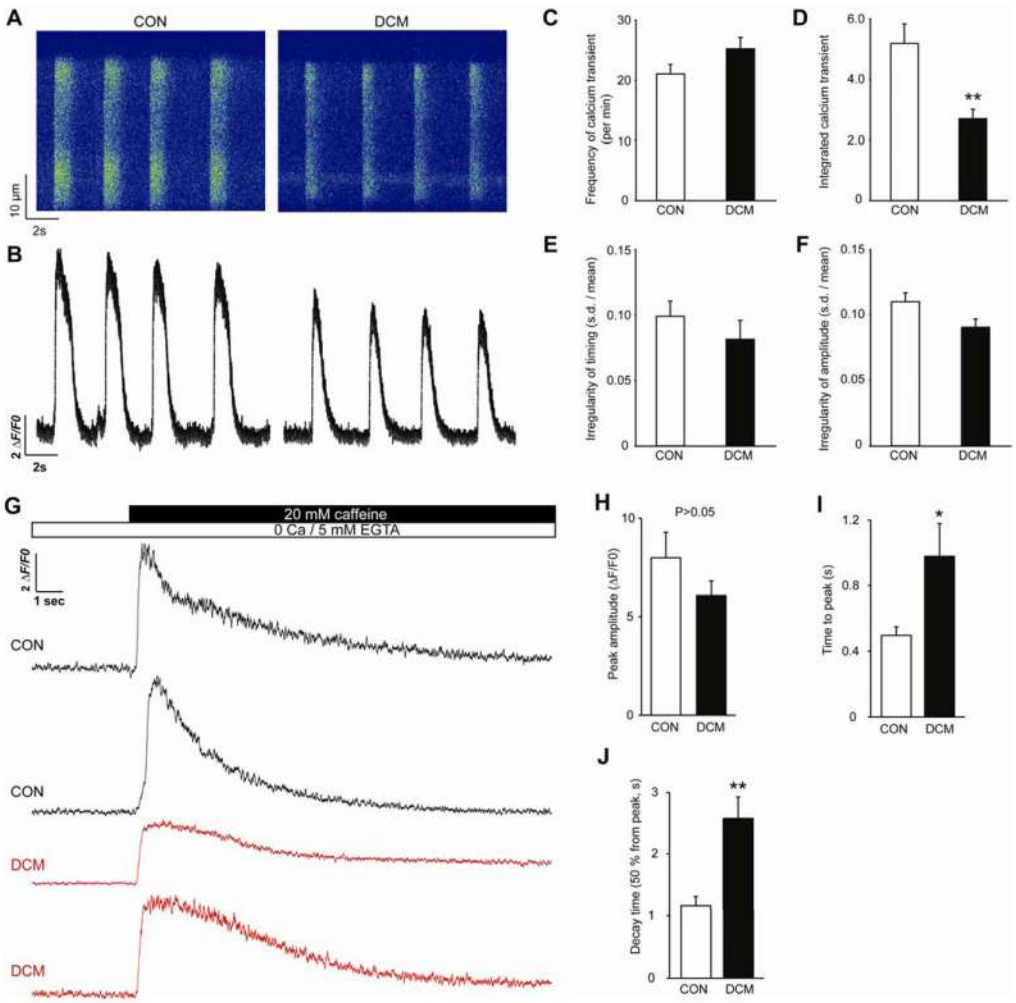

Figure 5. TNNT2 R173W DCM iPSC-CMs exhibited abnormal Ca^{2+} handling abilities

(A) Representative line-scan images and **(B)** spontaneous Ca^{2+} transients in control (left) and DCM iPSC-CMs (right). **(C)** Frequency of spontaneous Ca^{2+} transients in control and DCM iPSC-CMs. **(D)** Integration of $[Ca^{2+}]_i$ transients in control and DCM iPSC-CMs showed less Ca^{2+} released in each transient in DCM relative to control cells (control, n=87 cells; DCM, n=40 cells, **P=0.002). There were no significant differences in the irregularity of timing (standard deviation/mean) **(E)** or irregularity of amplitude **(F)** of the spontaneous Ca^{2+} transients between control and DCM cells. **(G–J)** Affected caffeine-evoked Ca^{2+} release in DCM iPSC-CMs. **(G)** Representative Ca^{2+} transients induced with 20 mM caffeine in Ca^{2+}-free condition in control and DCM iPSC-CMs (control, n=12, 2 iPSC lines, one each from 2 individuals; DCM, n=12, 2 iPSC lines, one each from 2 patients). **(H)** Peak amplitude of caffeine-evoked Ca^{2+} transients in control and DCM iPSC-CMs. The difference in the amplitude between control and DCM was observed but fail to reach statistical significance. **(I)** Time to peak in caffeine-evoked Ca^{2+} transients in control and DCM iPSC-CMs. **(J)** Decay time (50% from peak) in caffeine-evoked Ca^{2+} transients in control and DCM iPSC-CMs. Two-tailed Student's t-test (* $P < 0.05$, ** $P < 0.01$).

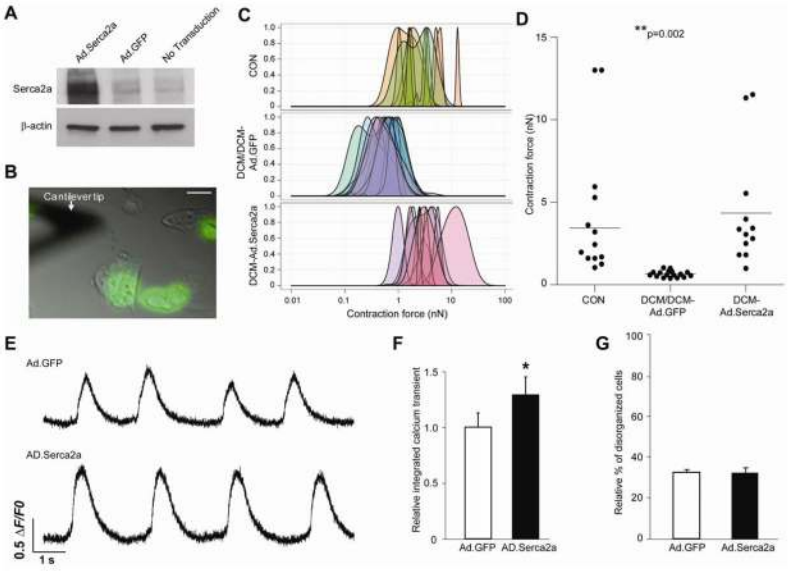

Figure 6. Over-expression of Serca2a restored contractility of TNNT2 R173W DCM iPSC-CMs

(A) Dot plots of mean contraction force of single CMs measured by AFM. One-way ANOVA analysis indicated that there was significant difference among the mean of all the groups (**p=0.002). Tukey's Multiple Comparison Test indicated that both control iPSC-CMs (n=13) (P=0.001) and Ad.Serca2a (n=12) (P=0.005) transduced DCM iPSC-CMs exhibited significantly stronger contraction force than that transduced by Ad.GFP (n=17). Ad.Serca2a transduced DCM iPSC-CMs showed comparable contraction force to that of the control iPSC-CMs (p=0.578). **(B)** Histograms of contraction forces of all the single iPSC-CMs measured by AFM over 100–400 beats. Over-expression of Serca2a significantly restored the contraction force of DCM iPSC-CMs to a level close to that of the controls. **(C)** Western blotting of Serca2a expression after adenoviral transduction of cells dissociated from iPSC beating EBs. Serca2a protein level was upregulated in cells transduced with Ad.Serca2a but not in cells transduced with Ad.GFP. **(D)** A representative image showing the AFM cantilever approaching GFP positive single beating CMs. Bar, 50 μm. **(E)** Representative spontaneous Ca^{2+} transients in single DCM iPSC-CMs transduced with Ad.GFP and Ad.Serca2a, respectively. **(F)** DCM iPSC-CMs transduced with Ad.Serca2a (n=22) exhibited increased global Ca^{2+} transients compared to cells transduced with Ad.GFP (n=14). (*p=0.04) (two-tailed Student's t-test). (**G**) Half decay time of Ca^{2+} transients in DCM iPSC-CMs transduced with Ad.Serca2a or with Ad.GFP. **(H)** Percentage of CMs with disorganized sarcomeric α-actinin staining pattern in single DCM iPSC-CMs with Ad.Serca2a (n=40) or Ad.GFP (n=40) over-expression. No significant difference was observed between the two groups (two-tailed Student's t-test). Data are presented as mean ±s.e.m.